Optical property – composition correlation in noble metal alloy nanoparticles studied with EELS

Kadkhodazadeh, Shima; Nugroho, Ferry Anggoro Ardy; Langhammer, Christoph; Beleggia, Marco; Wagner, Jakob Birkedal

Published in:
ACS Photonics

Link to article, DOI:
10.1021/acsphotonics.8b01791

Publication date:
2019

Document Version
Peer reviewed version

Optical property – composition correlation in noble metal alloy nanoparticles studied with EELS

Shima Kadkhodazadeh,*,† Ferry Anggoro Ardy Nugroho,‡ Christoph Langhammer,‡ Marco Beleggia,† Jakob B. Wagner,†

† DTU Nanolab, Technical University of Denmark, Kgs. Lyngby, 2800, Denmark
‡ Department of Physics, Chalmers University of Technology, Göteborg, 412 96, Sweden
*E-mail: shka@cen.dtu.dk

ABSTRACT: Noble metals are currently the most common building blocks in plasmonics and thus define the available range of optical properties. Their alloying provides a viable strategy to engineer new materials with a tunable range of optical responses. Despite this attractive prospect, the link between composition and optical properties of many noble metal alloys is still not well understood. Here, electron energy-loss spectroscopy is employed to systematically study AuAg and AuPd nanoparticles of varying compositions. The localized surface plasmons, the bulk plasmons and the permittivity functions of these two sets of alloys are investigated as functions of their composition. In the case of the more widely studied AuAg alloy system, good agreement is found with previous experimental and theoretical studies. The results on the less scrutinized AuPd system provide highly valuable experimental data that complements other experimental investigations and supports the development of theoretical models.

KEYWORDS: plasmonics, alloys, nanoparticles, electron energy-loss spectroscopy, optical properties, localized surface plasmons, permittivity function

Alloying has long been exploited as an avenue to tailor material properties by combining desirable traits of the constituent elements. In some cases, synergetic effects result in new interesting characteristics and/or the enhancement of the functionality of the alloy relative to its pure counterparts. In catalysis, for example, bimetallic alloy nanomaterials have shown superior catalytic activity for numerous reactions[1–3]. Alloys are also gaining interest in plasmonics, since tuning their composition provides an additional dial for manipulating the plasmonic response of nanostructures[4–10]. There, the precise control of a wide range of optical properties achieved by alloying has the potential to become a key ingredient for the viability of plasmonic structures in a range of applications that span from solar cells[11] to optical detectors[12–14], and metamaterials[15]. Furthermore, this strategy provides the prospect of gaining access to additional functionalities and characteristics, such as tailored catalytic activity and magnetism, which are relevant in plasmon mediated catalysis[16] and magnetoplasmonics[17], respectively. Additionally, in some cases, alloying can decrease the usage of precious metals such as gold in plasmonic devices. While the search of alternative plasmonic materials is expanding[18], noble metals, specifically gold and silver, are still the most common building blocks of plasmonic nanostructures. Gold, in particular, is attractive for many applications, due to its long-term chemical stability and biocompatibility. Pd is another interesting plasmonic material, particularly in the context of active plasmonics, where its optical properties are modulated in response to hydrogen exposure[19,20]. Taking advantage of alloying, recent studies on nanoplasmonic hydrogen sensors have demonstrated promising results for alloys of Pd with other noble metals[14,21,22].

Despite the significant potential outlined above, the optical properties of noble metal alloys are poorly understood. Among binary noble metal alloys, AuAg is studied the most[8,13,23–27] and a number of experimental and theoretical studies of the composition dependence of the complex permittivity function $\varepsilon_{\mathrm{AuAg}}(\omega)$ exist in the literature[6,23,26–29]. One of the key findings reported is

that $\varepsilon_{AuAg}(\omega)$ cannot be approximated as a weighted average of $\varepsilon_{Au}(\omega)$ and $\varepsilon_{Ag}(\omega)$, indicating a non-linear dependence of the permittivity function on the alloying ratio. Despite this important insight, the optical properties of other noble metal alloys are less heavily scrutinized[5–7,30–35]. In particular, experimental studies reporting or validating theoretically predicted alloy permittivity functions in many cases are needed. To shed light on these issues, we have employed electron energy-loss spectroscopy (EELS) to characterize the optical properties of two sets of nanofabricated disk-shaped noble metal alloy nanoparticles: AuAg and AuPd. EELS is a powerful technique for optical characterization of nanostructures due to its superior spatial resolution, which has played a key role in visualizing and understanding localized surface plasmon (LSPR) modes in nanostructures[36–44]. Another area where EELS has made a significant contribution is in accessing bulk losses, which also affect the optical properties[45]. Our investigation here includes probing the LSPR modes supported by the alloy nanoparticles, the characterization of the bulk losses, and the determination of the complex permittivity function as a function of alloy composition. The results demonstrate the role of alloying in tuning optical properties, where compositional changes as little as 10% result in distinct modifications in the spectral features recorded from the nanoparticles. Moreover, while the results confirm the non-linear dependence of the permittivity function of alloys on those of the constituent elements, very different trends are observed in the optical properties of AuAg and AuPd with varying composition. We interpret these differences in terms of the effect of the electronic structures of Ag and Pd on the Drude formulation of the permittivity function. Finally, the implications of the results for the plasmonic response of AuAg and AuPd nanostructures are discussed.

RESULTS

Arrays of AuAg and AuPd nanodisks with varying Au concentrations were fabricated on SiN_x membranes for STEM–EELS examination using hole-mask colloidal lithography and subsequent thermal annealing, following the method established by Nugroho et al.[10], which ensures the formation of homogeneous alloys[10,12] (Figure 1a). Interparticle distances larger than

3*R*, where *R* is the radius of the particles, were chosen in the samples to avoid near-field coupling and to prevent significant interaction between the plasmon modes of neighboring particles[46]. Representative annular dark-field (ADF) STEM images of the particles are shown in Figure 1b. For each composition, particles with a variety of microstructures, from single crystal to polycrystalline with different number of grains are observed (see Figure S2 in the Supporting Information, (SI)). However, no clear correlation between the particles' microstructure and the subsequent EELS measurements could be ascertained (Figure S3 in the SI).

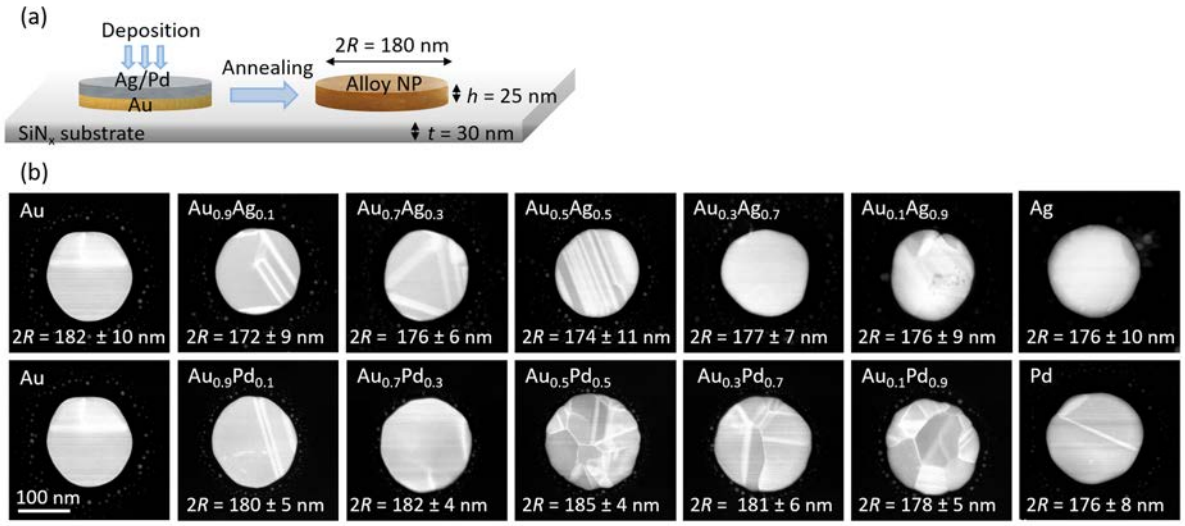

Figure 1. (a) Schematic depiction of the geometry of the alloy nanodisks on SiN_x TEM membranes together with the nanofabrication principle. (b) ADF STEM images of AuAg and AuPd nanoparticles of varying compositions. The average diameter of the particles along with the statistical errors are displayed on each images (10 different particles measured for each alloy composition).

Energy dispersive X-ray spectroscopy (EDS) analysis revealed that the particles have uniform chemical compositions, which is on average within ~4% of the nominal values[10] (Table S1). EELS was then used to probe their optical properties. Our investigation includes measurements in two specific configurations: (a) with the electron beam external to the particles and 5-10 nm away from their edges (so-called aloof configuration) and (b) with the beam passing through the center of the particles. The former probes the LSPR modes and the latter the bulk plasmon.

The results for AuAg and AuPd alloys of systematically varied compositions are shown in Figure 2.

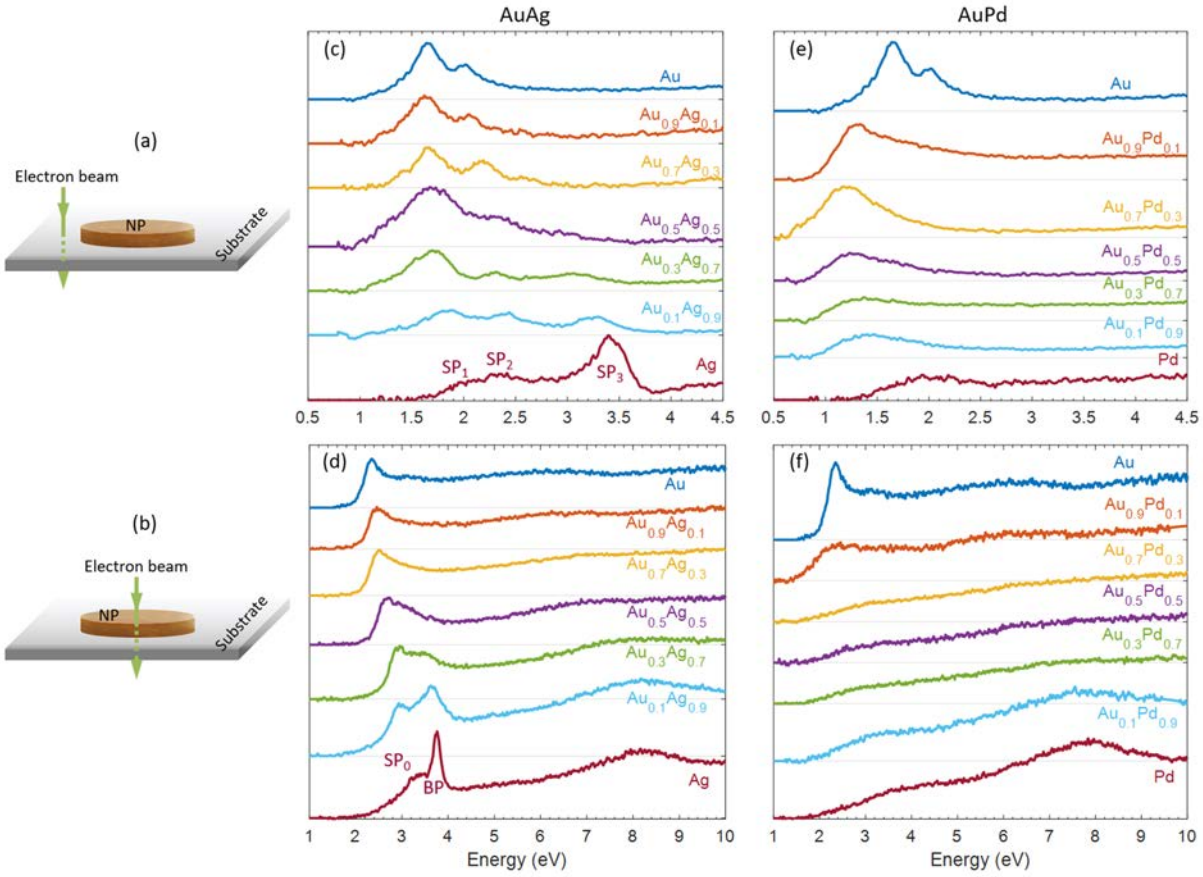

Figure 2. EEL spectra acquired from AuAg and AuPd nanoparticles, in two configurations: (a) with the electron beam positioned external to the particle and ~ 5 nm from its edge (aloof mode) and (b) with the electron beam traversing the center of the particle. The spectra recorded for AuAg alloy nanoparticles of systematically varying compositions in configurations (a) and (b) are plotted in (c) and (d), respectively, and those for AuPd nanoparticles in (e) and (f), respectively.

SURFACE EXCITATIONS. The LSPRs of the particles probed in the aloof configuration (Figure 2a) are presented in Figure 2c and e. At least two distinct peaks are observed in the spectrum recorded from the nanoparticle composed purely of Au. In contrast, the EEL spectrum recorded from the Ag contains at least three distinct peaks and that from Pd contains a single broad peak. Our results on Au and Ag nanoparticles are consistent with the literature[36,47,48]. Silver disks of comparable dimensions have been shown to support at least three LSPR modes, when the electron beam is positioned in a similar configuration to Figure 2a[36]. These modes,

identified as the dipole, quadruple and hexapole LSPRs, are marked in Figure 2c with SP_1–SP_3, respectively.

Increasing the Au content of the AuAg alloy nanoparticles results in shifts of the spectral positions (location of maxima on the energy axis) of the LSPRs, as well as changes in spectral widths (related to the damping of the plasmons[44]). The number of modes observed in the EEL spectra in Figure 2c has a dependence on composition, as only the dipole and quadruple LSPRs can be resolved for Au concentrations larger than 0.7. This is most likely due to increased damping arising from the onset of interband transitions. In the case of AuPd, similar to Pd, only a single broad LSPR is observed (Figure 2e). Besides the above mentioned modes, Schmidt *et al.* [36] have identified dark surface plasmons with radial symmetry in Ag nanoparticles, which couple to the electron beam when the beam passes through the nanoparticles. Such a dark mode, known as the breathing or zero-order mode, is excited in configuration (b) at ~3 eV for our Ag particles (marked as SP_0 in Figure 2d). Similar to the dipole, quadruple and hexapole modes, the breathing mode redshifts with increasing Au content in the AuAg alloy. The breathing mode in AuAg cannot be resolved for Au concentrations higher than 0.7 and is not resolved for any of the AuPd nanoparticles.

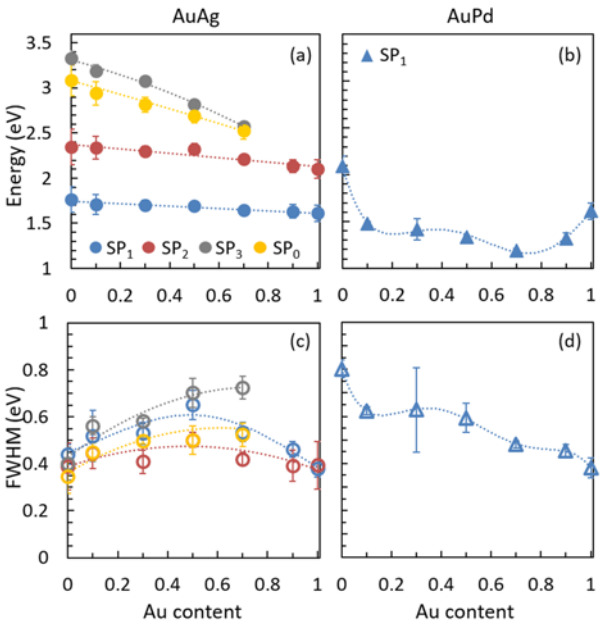

Figure 3. The spectral position of the dipole (SP_1), quadruple (SP_2), hexapole (SP_3) and breathing (SP_0) LSPR modes as a function of the Au fractional content in (a) AuAg and (b) AuPd nanoparticles. The FWHM of the corresponding modes are plotted in (c) for AuAg and in (d) for AuPd. The displayed values for each composition are averaged over measurements from 5-10 particles and the error bars represent the standard deviation of the measurements.

The spectral positions and line-widths (full-width at half-maximum (FWHM)) of the LSPRs of AuAg and AuPd nanoparticles as a function of their Au fractions are summarized in Figure 3. Comparing the composition dependence of the LSPRs in the two sets of alloys, unequivocal differences are observed: all the LSPRs detected for the AuAg particles redshift with increasing Au composition and, in most cases, linearly with the Au content of the alloy (Figure 3a). The same trend has been observed for AuAg truncated nanospheres[24]. In contrast, the spectral position of the LSPR in AuPd particles shows a highly non-linear dependence on alloy composition, with local minima and a local maximum (Figure 3b). This is in very good agreement with optical measurements of the LSPRs in corresponding ensembles of AuPd alloy nanoparticles[10]. Our measurements also reveal a very different trend in the linewidth of the LSPRs in AuAg compared to AuPd. Specifically, in the AuAg system, the linewidths of SP_1 and SP_2 exhibit a maximum at 50% Au composition, whereas the linewidths of SP_3 and SP_0

(for the compositions they are resolved) increase with increasing Au content. In the AuPd system the largest linewidth is observed for pure Pd.

BULK EXCITATIONS. The EEL spectra acquired in the configuration of Figure 2d, were used to determine the energy and line-width of the bulk plasmon (BP) in AuAg and AuPd alloys (Figure 2e-f). When only bulk losses are excited, the bulk plasmon is the most intense feature in the energy-loss spectrum[49]. This was used to distinguish between the BP and single electron transitions also present in the spectra in Figure 2. In the case of AuPd alloys, it was necessary to subtract the signal from the substrate in order to distinguish between the BP and other spectral features (Figure S4 in the SI). For the AuAg system, the BP was distinguished from the breathing surface mode based on the criterion that it occurs at an energy higher than the surface plasmons. The energy of the BP measured here for pure Au, Ag and Pd are consistent with the EELS measurements reported elsewhere[50–53]. The spectral positions and linewidths of the BP in AuAg and AuPd alloys as functions of their Au content are summarized in Figure 4. Similar to the surface excitations, the bulk plasmon energy in AuPd exhibits a highly non-linear dependence on the alloy composition. In contrast, in AuAg the BP energy monotonically decreases with increasing the Au content of the alloy and can be adequately described by a second order polynomial function.

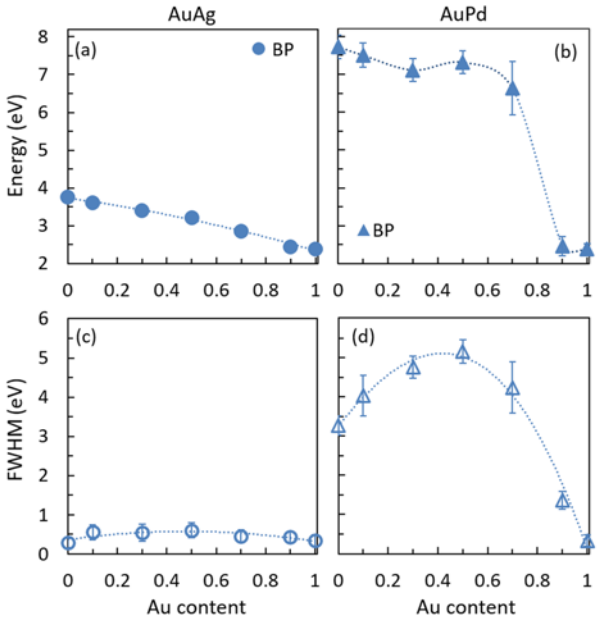

Figure 4. The spectral positions of the bulk plasmon in (a) AuAg and (b) AuPd alloys, as a function of their Au fractional content. The FWHM of the bulk plasmon of the alloys are plotted in (c) for AuAg and in (d) for AuPd.

KRAMERS-KRONIG ANALYSIS OF ALLOY PERMITTIVITY FUNCTION. To derive the frequency-dependent real, $\varepsilon_1(\omega)$, and imaginary, $\varepsilon_2(\omega)$, parts of the complex permittivity function of the alloys, we have applied the Kramers-Kronig analysis method[49] to our EELS data. The resulting complex permittivity function of AuAg alloys of different compositions are shown in Figure 5 alongside the analytical model developed by Rioux *et al.*[29]. Small differences between the two data sets, including an underestimation of $\varepsilon_1(\omega)$ and $\varepsilon_2(\omega)$ values in the EELS data and a slight redshift of the main features can be noticed. Both of these differences can be a consequence of the larger momentum transfer by the electrons in EELS compared to photons in optics[49]. However, in general, there is good agreement between our experimental data and the theoretical model, as the key features are consistent in the two sets of data and they follow the same trends with changes in composition. Thus, we conclude that our approach is a valid method for extracting the key characteristics of the complex permittivity function and scrutinizing its evolution with changes in composition.

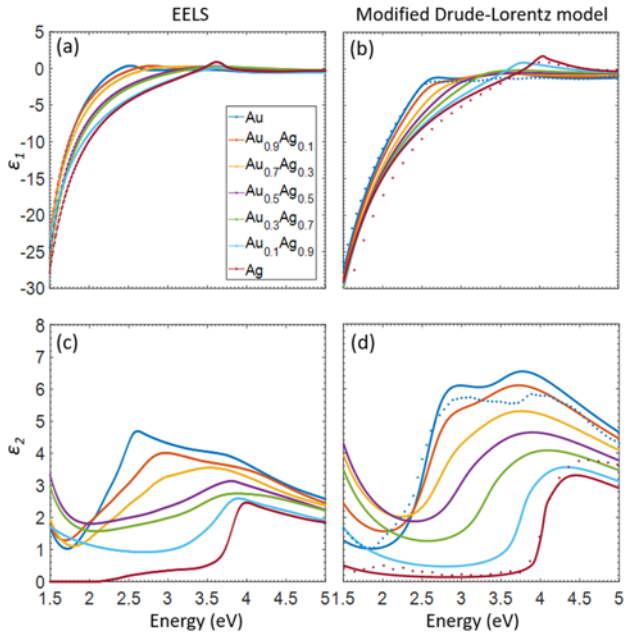

Figure 5. The real, $\varepsilon_1(\omega)$, and imaginary, $\varepsilon_2(\omega)$, components of the complex permittivity function of AuAg alloys as a function of systematically varied composition obtained by ((a) and (c)) applying the Kramers-Kronig method to the experimental EEL spectra, and ((b) and (d)) based on the modified Drude-Lorentz model developed by Rioux *et al*.[29]. The dotted lines in (b) and (d) depict the experimentally measured $\varepsilon_1(\omega)$ and $\varepsilon_2(\omega)$ for pure Au and Ag, as reported by Johnson and Christy[54].

Our EELS measurements of $\varepsilon_1(\omega)$ and $\varepsilon_2(\omega)$ in AuPd alloys are presented in Figure 6. Due to the lack of systematic studies of the permittivity of AuPd alloys in the literature, only the optically measured permittivity functions of pure Au and Pd are plotted for comparison, both of which agree reasonably well with our experimental data.

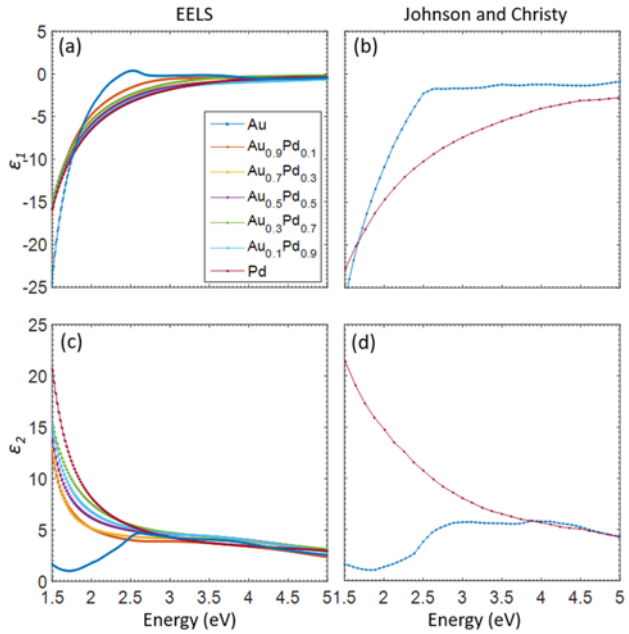

Figure 6. The real, $\varepsilon_1(\omega)$, and imaginary, $\varepsilon_2(\omega)$, components of the complex permittivity function of AuPd alloys as a function of systematically varied composition obtained by ((a) and (c)) applying Kramers-Kronig analysis to the experimental EEL spectra, and ((b) and (d)) of pure Au and Pd, as reported by Johnson and Christie[54,55].

DISCUSSION

Our results demonstrate the wide tunability of the optical properties through alloying and their non-trivial dependence on alloy composition. Interestingly, very different behaviors are observed for AuAg and AuPd alloys, as we further discuss and analyze below.

The Drude formulation of the permittivity function of a metal is given by[56]:

$$\varepsilon(\omega) = \varepsilon_\infty - \frac{\Omega_p^2}{\omega^2 + i\omega\Gamma}, \quad (1)$$

with

$$\Omega_p = \sqrt{\frac{ne^2}{\varepsilon_0 m_e}} \quad (2)$$

where, ε_∞ is the bound electrons contribution, Ω_p is the free-electron bulk plasmon frequency with damping Γ, n is the free electron density, m_e is the electron mass, e is the electron charge and ε_0 is the permittivity of free space. In a strictly free-electron model, Γ is negligible and $\varepsilon_\infty = 1$. However, additional screening induced by bound valence electrons of the positive ion cores results in $\varepsilon_\infty > 1$ and damping gives larger Γ. Applying the criterion $\varepsilon_1(\omega_p) = 0$ to Equation (1),

the bulk plasmon of a material, ω_p, is found to be $\omega_p = \frac{\Omega_p}{\sqrt{\varepsilon_\infty}}$, which corresponds to the bulk plasmon values measured with EELS here. Figure 7 shows ε_∞ of the alloys as a function of their Au content calculated using our experimentally measured ω_p and known Ω_p values. Two sets of Ω_p values were used here: i) Ω_p values taken directly from the literature and depicted with circles in Figure 7a-b. In the case of AuPd alloys, only a reference Ω_p value for $Au_{0.5}Pd_{0.5}$ could be found in the literature[4] and inaccuracies may be present there, since their Ω_p value for pure Pd diverges significantly from that of Johnson and Christy[55] (Figure 7b). ii) Ω_p calculated according to Equation (2), and estimating the free-electron density by $n = \frac{zN_A\rho}{A}$, where N_A is the Avogadro constant, ρ is the material density, z is the valency of the material and A is the atomic weight (depicted with squares in Figure 7a-b). The composition dependence of the density of AuAg and AuPd is shown in Figure S5 in the SI. Interestingly, Ω_p in AuAg in both the model developed by Rioux *et al*[29] and calculated from Equation (2) shows a second order dependence on the Au content of the alloy, similar to what was observed for ω_p of AuAg in Figure 4.

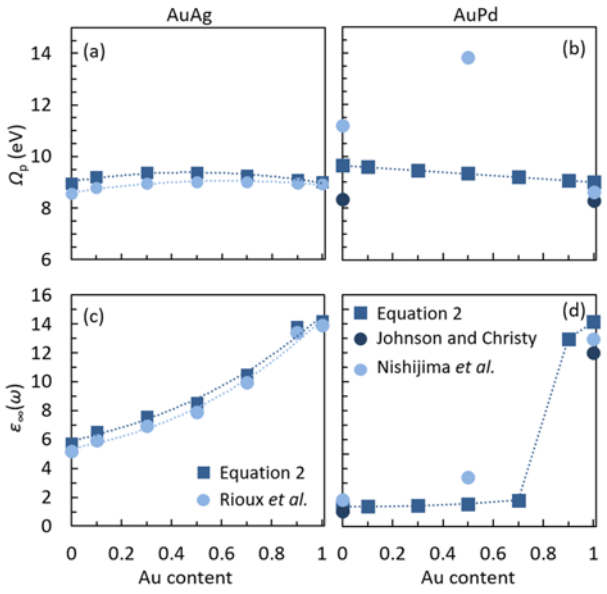

Figure 7. Free-electron bulk plasmon frequency, Ω_p, of (a) AuAg and (b) AuPd taken from the cited references in the literature[4,29,54,55] (circles) and calculated using Equation (2) (squares). Bound electrons contribution, $\boldsymbol{\varepsilon_\infty = \left(\frac{\Omega_p}{\omega_p}\right)^2}$, of (c) AuAg and (d) AuPd alloys determined using the two sets of Ω_p values in (a) and (b) and the experimentally measured ω_p values in Figure 4.

We obtain $\varepsilon_{\infty Au} \approx 12$, $\varepsilon_{\infty Ag} \approx 5$ and $\varepsilon_{\infty Pd} \approx 1$ from the above procedure. $\varepsilon_{\infty Pd} \approx 1$ gives the better known Drude description, $\varepsilon(\omega) = 1 - \frac{\Omega_p^2}{\omega^2 + i\Gamma\omega}$. Our ε_∞ values for Au and Ag are in reasonable agreement with those reported by de Abajo ($\varepsilon_{\infty Au}$=9.5 and $\varepsilon_{\infty Ag}$= 4)[45]. Such large values of ε_∞ indicates significant screening of the conduction electrons. Au and Ag atoms have very similar electron configurations, in that both have full *d* orbitals followed by a singly filled *s* orbital in their outer shells (Ag: [Kr] $4d^{10}$ $5s^1$ and Au: [Xe] $4f^{14}$ $5d^{10}$ $6s^1$). It is the screening induced on the *s* electrons by the bound *d* electrons, which manifests itself in large ε_∞ values in the Drude description of their permittivity functions. In AuAg alloys, ε_∞ monotonically increases with increasing Au content (Figure 7c), suggesting similar electronic structure of the alloy. In contrast, Pd has a rather different electron configuration, with its outer shell consisting of a full set of *d* orbitals (Pd: [Kr] $4d^{10}$). Although plasmon excitations in Pd are highly damped (due to the bound electrons in its outer shell), the screening induced on these electrons is negligible. The results in Figure 7d suggests an abrupt transition in the Drude description of $\varepsilon_{AuPd}(\omega)$ with increasing Au content at $Au_{0.7}Pd_{0.3}$ from what resembles Pd to Au. X-ray spectroscopy studies of AuPd alloys have suggested considerably stronger hybridization of the Au 5d and Pd 4d states in the Pd-rich alloys compared to Au-rich alloys, which can explain this abrupt transition[57].

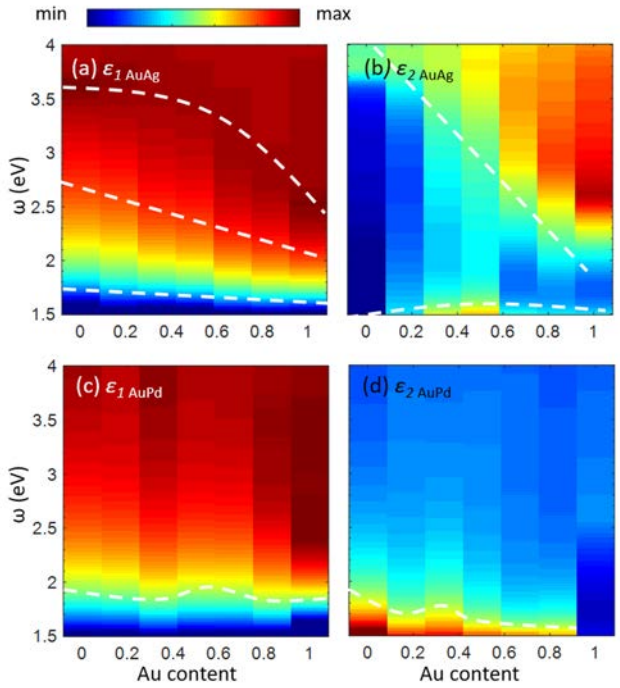

Figure 8. Maps of $\varepsilon_1(\omega)$ and $\varepsilon_2(\omega)$ obtained from applying the Kramers-Kroning method to the EELS data as a function of Au content of the AuAg and AuPd alloys.

Now examining the evolvement of the complex permittivity function of the alloys as a function of their composition, plotted in Figure 8, we discuss a few practical implications of the obtained results. In general, the resonance frequency of plasmon excitations in metals is largely dependent on $\varepsilon_1(\omega)$, while $\varepsilon_2(\omega)$ is related to absorption and losses in a material[56]. In the case of AuAg, $\varepsilon_1(\omega)$ increases almost linearly with increasing Au content in the alloys in the near infrared and the visible light range (Figure 8a). The slope of ε_{1AuAg} vs. Au fraction of the alloy appears to increase at higher energies. Both of these trends are consistent with our measurements in Figure 3a, where a close to linear relationship between the LSPR energies of the AuAg nanoparticles and their Au content and with a larger slope for the higher energy LSPR modes was found. A more complex behavior is seen for ε_{2AuAg} (Figure 8b): below ~2.2 eV, ε_{2AuAg} vs. Au content reaches a maximum at $Au_{0.5}Ag_{0.5}$, while above ~2.2 eV, ε_{2AuAg} increases monotonically with increasing Au content (at higher energies it also deviates from a linear to an arched profile). Again, the same pattern is reflected in the FWHM measurement of the LSPR modes in AuAg nanoparticles in Figure 3c. We can, therefore, conclude that below ~2.2 eV

alloying Au and Ag results in higher losses compared to both metals. Above ~2.2 eV, however, AuAg alloys have lower losses compared to pure Au. Losses in AuAg are always higher relative to pure Ag, although, improved chemical stability can be achieved through alloying with Au. In the case of AuPd alloys, ε_{1AuPd} follows a similar highly non-linear dependence on alloy composition (Figure 8c), to that observed for the dipole LSPR mode in Figure 3b. ε_{2AuPd} in Figure 3d shows significantly lower values at $\omega < 2.5$ eV for pure Au and larger values for pure Pd, in particular at $\omega < 1.8$ eV compared to AuPd alloys. The results indicate that alloying Pd with Au is an effective strategy for reducing optical losses. Losses in AuPd alloys in the near infrared and visible range remain generally higher than in pure Au. However, incorporation of Pd can offer additional functionalities, for example in hydrogen sensing and active plasmonics.

SUMMARY AND CONCLUSIONS

In summary, we have utilized EELS to probe the LSPRs and the bulk plasmons of AuAg and AuPd nanoparticles with varying Au content and to derive their complex permittivity functions. Our analysis reveals very contrasting behaviors of these parameters as functions of composition in AuAg and AuPd alloys. In the case of AuAg nanoparticles, the spectral position of the LSPRs has approximately a linear dependence on the Au content of the alloy, while the spectral position of LSPRs in AuPd nanoparticles shows a highly non-linear dependence on Au content. The linewidths of the LSPRs in these two sets of alloys also follow very different profiles. The BP energy vs. composition in AuAg follows closely a second order polynomial profile, while that in AuPd is highly non-linear and shows a sharp decrease at ~ $Au_{0.7}Pd_{0.3}$ with increasing Au content. These differences are reflected in the permittivity functions derived for the alloys, and are discussed in terms of the electronic structures of Ag and Pd. Overall, the results demonstrate the wide tunability of the LSPRs with composition, highlighting that alloying can give access to a new palette of optical properties that is yet unexplored.

METHODS

NANOFABRICATION. AuAg and AuPd alloy nanodisks were fabricated on in-house-made TEM windows[58] following the procedures described in detail elsewhere[10,12], based on layer-by-layer deposition of the metallic constituent through a pre-fabricated mask produced by hole-mask colloidal lithography. Due to the presence of a PMMA thin film between the support (TEM membrane) and the polystyrene colloidal particles used to form the self-assembled mask, the structural integrity of the TEM membrane is maintained throughout the fabrication process. Homogeneous alloying was achieved by annealing at 500 ^{o}C for 24 h in 4% H_2 in Ar at atmospheric pressure.

ELECTRON MICROSCOPY. The alloy nanoparticles were examined using a FEI Titan TEM instrument fitted with a monochromator, aberration correction on the probe forming lenses and a Gatan GIF Tridium 865 spectrometer. The microscope was operated at 120kV accelerating voltage and with the monochromator excited, giving spatial and energy resolutions of ~0.4 nm and ~0.15 eV, respectively. The convergence angle of the electron probe and the collection inner angle of the ADF images were 25 mrad and 27 mrad, respectively. The EEL spectra were recorded with the dispersion of 0.01 eV per channel, acquisition time of ~ 50 and spectrometer collection angle of 27 mrad. The recorded spectra were analyzed after (Fourier-log) deconvolution[49] of the zero-loss peak after power-law fitting of its tail (Figure S6 in the SI). The LSPRs and BPs were fitted with Gaussian models in order to estimate their spectral positions and widths. The Kramers-Kronig analysis was carried out using the Gatan Digital Micrgraph software.

SUPPLEMENTARY INFORMATION

Supporting Information containing EDS chemical composition analysis of the nanoparticles, the origin of the contrast in the ADF images, particle microstructure vs. BP and LSPR energy correlations, BP determination in AuPd alloys, density of AuAg and AuPd alloys vs.

composition and an example of the Fourier-log deconvolution applied to the EEL spectra accompanies this paper.

AUTHOR INFORMATION

Corresponding author:

*E-mail: shka@dtu.dk

ACKNOWLEDGEMENTS

We are grateful to Radu Malureanu and Søren Raza for fruitful discussions. SK, MB and JBW acknowledge A. P Møller and Christine Mc-Kinney Møller for their contribution towards the establishment of the electron microscopy center at the Technical University of Denmark. FAAN and CL acknowledge support from the Knut and Alice Wallenberg Foundation (project 2016.0210).

REFERENCES

(1) Liu, X.; Wang, D.; Li, Y. Synthesis and Catalytic Properties of Bimetallic Nanomaterials with Various Architectures. *Nano Today* **2012**, *7*, 448–466.

(2) Wang, D.; Li, Y. Bimetallic Nanocrystals: Liquid-Phase Synthesis and Catalytic Applications. *Adv. Mater.* **2011**, *23*, 1044–1060.

(3) Jiang, H. L.; Xu, Q. Recent Progress in Synergistic Catalysis over Heterometallic Nanoparticles. *J. Mater. Chem.* **2011**, *21*, 13705–13725.

(4) Nishijima, Y.; Hashimoto, Y.; Seniutinas, G.; Rosa, L.; Juodkazis, S. Engineering Gold Alloys for Plasmonics. *Appl. Phys. A Mater. Sci. Process.* **2014**, *117*, 641–645.

(5) Cortie, M. B.; McDonagh, A. M. Synthesis and Optical Properties of Hybrid and Alloy Plasmonic Nanoparticles. *Chem. Rev.* **2011**, *111*, 3713–3735.

(6) Gong, C.; Leite, M. S. Noble Metal Alloys for Plasmonics. *ACS Photonics* **2016**, *3*, 507–513.

(7) Xu, Z.; Lai, E.; Yang, S. H.; Hamad-Schifferli, K. Compositional Dependence of the Stability of AuCu Alloy Nanoparticles. *Chem. Commun.* **2012**, *48*, 5626–5628.

(8) Hashimoto, Y.; Seniutinas, G.; Balcytis, A.; Juodkazis, S.; Nishijima, Y. Au-Ag-Cu Nano-Alloys: Tailoring of Permittivity. *Sci. Rep.* **2016**, *6*, 1–9.

(9) Gong, C.; Kaplan, A.; Benson, Z. A.; Baker, D. R.; McClure, J. P.; Rocha, A. R.; Leite, M. S. Band Structure Engineering by Alloying for Photonics. *Adv. Opt. Mater.* **2018**, *6*, 1–7.

(10) Nugroho, F. A. A.; Iandolo, B.; Wagner, J. B.; Langhammer, C. Bottom-Up Nanofabrication of Supported Noble Metal Alloy Nanoparticle Arrays for Plasmonics. *ACS Nano* **2016**, *10*, 2871–2879.

(11) Xu, Q.; Liu, F.; Liu, Y.; Cui, K.; Feng, X.; Zhang, W.; Huang, Y. Broadband Light Absorption Enhancement in Dye-Sensitized Solar Cells with Au-Ag Alloy Popcorn Nanoparticles. *Sci. Rep.* **2013**, *3*, 2–8.

(12) Wadell, C.; Nugroho, F. A. A.; Lidström, E.; Iandolo, B.; Wagner, J. B.; Langhammer, C. Hysteresis-Free Nanoplasmonic Pd–Au Alloy Hydrogen Sensors. *Nano Lett.* **2015**, *15*, 3563–3570.

(13) Gao, C.; Hu, Y.; Wang, M.; Chi, M.; Yin, Y. Fully Alloyed Ag/Au Nanospheres: Combining the Plasmonic Property of Ag with the Stability of Au. *J. Am. Chem. Soc.* **2014**, *136*, 7474–7479.

(14) Nugroho, F. A. A.; Darmadi, I.; Zhdanov, V. P.; Langhammer, C. Universal Scaling and Design Rules of Hydrogen-Induced Optical Properties in Pd and Pd-Alloy Nanoparticles. *ACS Nano* **2018**, *12*, 9903–9912.

(15) Kim, J.; Naik, G. V.; Gavrilenko, A. V.; Dondapati, K.; Gavrilenko, V. I.; Prokes, S. M.; Glembocki, O. J.; Shalaev, V. M.; Boltasseva, A. Optical Properties of Gallium-Doped Zinc Oxide-a Low-Loss Plasmonic Material: First-Principles Theory and Experiment. *Phys. Rev. X* **2014**, *3*, 1–9.

(16) Aslam, U.; Rao, V. G.; Chavez, S.; Linic, S. Catalytic Conversion of Solar to Chemical Energy on Plasmonic Metal Nanostructures. *Nat. Catal.* **2018**, *1*, 656–665.

(17) Maksymov, I. S. Magneto-Plasmonic Nanoantennas: Basics and Applications. *Rev. Phys.* **2016**, *1*, 36–51.

(18) West, P. R.; Ishii, S.; Naik, G. V.; Emani, N. K.; Shalaev, V. M.; Boltasseva, A. Searching for Better Plasmonic Materials. *Laser Photonics Rev.* **2010**, *4*, 795–808.

(19) Jiang, N.; Zhuo, X.; Wang, J. Active Plasmonics: Principles, Structures, and Applications. *Chem. Rev.* **2018**, *118*, 3054–3099.

(20) Wadell, C.; Syrenova, S.; Langhammer, C. Plasmonic Hydrogen Sensing with Nanostructured Metal Hydrides. *ACS Nano* **2014**, *8*, 11925–11940.

(21) Matuschek, M.; Singh, D. P.; Jeong, H. H.; Nesterov, M.; Weiss, T.; Fischer, P.; Neubrech, F.; Liu, N. Chiral Plasmonic Hydrogen Sensors. *Small* **2018**, *14*, 1–7.

(22) Nugroho, F. A. A.; Eklund, R.; Nilsson, S.; Langhammer, C. A Fiber-Optic Nanoplasmonic Hydrogen Sensor *via* Pattern-Transfer of Nanofabricated PdAu Alloy Nanostructures. *Nanoscale* **2018**, *10*, 20533–20539.

(23) Moskovits, M.; Srnová-loufová, I.; Vlková, B. Bimetallic Ag-Au Nanoparticles: Extracting Meaningful Optical Constants from the Surface-Plasmon Extinction Spectrum. *J. Chem. Phys.* **2002**, *116*, 10435–10446.

(24) Wu, Y.; Li, G.; Cherqui, C.; Bigelow, N. W.; Thakkar, N.; Masiello, D. J.; Camden, J. P.; Rack, P. D. Electron Energy Loss Spectroscopy Study of the Full Plasmonic Spectrum of Self-Assembled Au-Ag Alloy Nanoparticles: Unraveling Size, Composition, and Substrate Effects. *ACS Photonics* **2016**, *3*, 130–138.

(25) Shore, M. S.; Wang, J.; Johnston-Peck, A. C.; Oldenburg, A. L.; Tracy, J. B. Synthesis of Au(Core)/Ag(Shell) Nanoparticles and Their Conversion to AuAg Alloy Nanoparticles. *Small* **2011**, *7*, 230–234.

(26) Link, S.; Wang, Z. L.; El-Sayed, M. A. Alloy Formation of Gold−Silver Nanoparticles and the Dependence of the Plasmon Absorption on Their Composition. *J. Phys. Chem. B* **1999**, *103*, 3529–3533.

(27) Gaudry, M.; Lermé, J.; Cottancin, E.; Pellarin, M.; Vialle, J. L.; Broyer, M.; Prével, B.; Treilleux, M.; Mélinon, P. Optical Properties of (AuxAg1-x) Clusters Embedded in Alumina: Evolution with Size and Stoichiometry. *Phys. Rev. B - Condens. Matter Mater. Phys.* **2001**, *64*, 1–7.

(28) Peña-Rodríguez, O.; Caro, M.; Rivera, A.; Olivares, J.; Perlado, J. M.; Caro, A. Optical Properties of Au-Ag Alloys: An Ellipsometric Study. *Opt. Mater. Express* **2014**, *4*, 403.

(29) Rioux, D.; Vallières, S.; Besner, S.; Muñoz, P.; Mazur, E.; Meunier, M. An Analytic Model for the Dielectric Function of Au, Ag, and Their Alloys. *Adv. Opt. Mater.* **2014**, *2*, 176–182.

(30) Bansal, A.; Sekhon, J. S.; Verma, S. S. Scattering Efficiency and LSPR Tunability of Bimetallic Ag, Au, and Cu Nanoparticles. *Plasmonics* **2014**, *9*, 143–150.

(31) Chen, J.; Wiley, B.; McLellan, J.; Xiong, Y.; Li, Z. Y.; Xia, Y. Optical Properties of Pd- Ag and Pt- Ag Nanoboxes Synthesized via Galvanic Replacement Reactions. *Nano Lett.* **2005**, *5*, 2058.

(32) Blaber, M. G.; Arnold, M. D.; Ford, M. J. A Review of the Optical Properties of Alloys and Intermetallics for Plasmonics. *J. Phys. Condens. Matter* **2010**, *22*, 143201.

(33) Jing, H.; Wang, H. Structural Evolution of Ag-Pd Bimetallic Nanoparticles through Controlled Galvanic Replacement: Effects of Mild Reducing Agents. *Chem. Mater.* **2015**, *27*, 2172–2180.

(34) Blaber, M. G.; Arnold, M. D.; Ford, M. J. Optical Properties of Intermetallic Compounds from First Principles Calculations: A Search for the Ideal Plasmonic Material. *J. Phys. Condens. Matter* **2009**, *21*.

(35) Motl, N. E.; Ewusi-annan, E.; Sines, I. T.; Jensen, L.; Schaak, R. E. Au-Cu Alloy Nanoparticles with Tunable Compositions and Plasmonic Properties: Experimental Determination of Composition and Correlation with Theory. *J. Phys. Chem. C* **2010**,

114, 19263–19269.

(36) Schmidt, F. P.; Ditlbacher, H.; Hohenester, U.; Hohenau, A.; Hofer, F.; Krenn, J. R. Dark Plasmonic Breathing Modes in Silver Nanodisks. *Nano Lett.* **2012**, *12*, 5780–5783.

(37) Nicoletti, O.; de la Peña, F.; Leary, R. K.; Holland, D. J.; Ducati, C.; Midgley, P. A. Three-Dimensional Imaging of Localized Surface Plasmon Resonances of Metal Nanoparticles. *Nature* **2013**, *502*, 80–84.

(38) Rossouw, D.; Couillard, M.; Vickery, J.; Kumacheva, E.; Botton, G. A. Multipolar Plasmonic Resonances in Silver Nanowire Antennas Imaged with a Subnanometer Electron Probe. *Nano Lett.* **2011**, *11*, 1499–1504.

(39) Ringe, E.; Desantis, C. J.; Collins, S. M.; Duchamp, M.; Dunin-Borkowski, R. E.; Skrabalak, S. E.; Midgley, P. A. Resonances of Nanoparticles with Poor Plasmonic Metal Tips. *Sci. Rep.* **2015**, *5*, 1–9.

(40) Colliex, C.; Kociak, M.; Stéphan, O. Electron Energy Loss Spectroscopy Imaging of Surface Plasmons at the Nanometer Scale. *Ultramicroscopy* **2015**, *162*, A1–A24.

(41) Bosman, M.; Keast, V. J.; Watanabe, M.; Maaroof, A. I.; Cortie, M. B. Mapping Surface Plasmons at the Nanometre Scale with an Electron Beam. *Nanotechnology* **2007**, *18*.

(42) Ye, E.; Regulacio, M. D.; Bharathi, M. S.; Pan, H.; Lin, M.; Bosman, M.; Win, K. Y.; Ramanarayan, H.; Zhang, S. Y.; Loh, X. J.; et al. An Experimental and Theoretical Investigation of the Anisotropic Branching in Gold Nanocrosses. *Nanoscale* **2016**, *8*, 543–552.

(43) Tan, S. F.; Lin, W.; Yang, J. K. W.; Bai, P.; Bosman, M.; Nijhuis, C. A. Quantum Plasmon Resonances Controlled by Molecular Tunnel Junctions. *Science (80-.).* **2014**, *343*, 1496–1498.

(44) Bosman, M.; Ye, E.; Tan, S. F.; Nijhuis, C. A.; Yang, J. K. W.; Marty, R.; Mlayah, A.;

Arbouet, A.; Girard, C.; Han, M.-Y. Surface Plasmon Damping Quantified with an Electron Nanoprobe. *Sci. Rep.* **2013**, *3*, 1312.

(45) García De Abajo, F. J. Optical Excitations in Electron Microscopy. *Rev. Mod. Phys.* **2010**, *82*, 209–275.

(46) Kadkhodazadeh, S.; de Lasson, J. R.; Beleggia, M.; Kneipp, H.; Wagner, J. B.; Kneipp, K. Scaling of the Surface Plasmon Resonance in Gold and Silver Dimers Probed by EELS. *J. Phys. Chem. C* **2014**, *118*, 5478–5485.

(47) Schmidt, F. P.; Ditlbacher, H.; Hofer, F.; Krenn, J. R.; Hohenester, U. Morphing a Plasmonic Nanodisk into a Nanotriangle. *Nano Lett.* **2014**, *14*, 4810–4815.

(48) Forcherio, G. T.; DeJarnette, D.; Benamara, M.; Roper, D. K. Electron Energy Loss Spectroscopy of Surface Plasmon Resonances on Aberrant Gold Nanostructures. *J. Phys. Chem. C* **2016**, *120*, 24950–24956.

(49) Egerton, R. F. *Electron Energy-Loss Spectroscopy in the Electron Microscope*, 3rd ed.; Plenum Press: New York, 2011.

(50) Koh, A. L.; Bao, K.; Khan, I.; Smith, W. E.; Kothleitner, G.; Nordlander, P.; Maier, S. A.; McComb, D. W. Electron Energy-Loss Spectroscopy (EELS) of Surface Plasmons in Single Silver Nanoparticles and Dimers: Influence of Beam Damage and Mapping of Dark Modes. *ACS Nano* **2009**, *3*, 3015–3022.

(51) Kadkhodazadeh, S.; Christensen, T.; Beleggia, M.; Mortensen, N. A.; Wagner, J. B. The Substrate Effect in Electron Energy-Loss Spectroscopy of Localized Surface Plasmons in Gold and Silver Nanoparticles. *ACS Photonics* **2017**, *4*, 251–261.

(52) Baldi, A.; Narayan, T. C.; Koh, A. L.; Dionne, J. A. In Situ Detection of Hydrogen-Induced Phase Transitions in Individual Palladium Nanocrystals. *Nat. Mater.* **2014**, *13*, 1143–1148.

(53) Raza, S.; Stenger, N.; Pors, A.; Holmgaard, T.; Kadkhodazadeh, S.; Wagner, J. B.; Pedersen, K.; Wubs, M.; Bozhevolnyi, S. I.; Mortensen, N. A. Extremely Confined

Gap Surface-Plasmon Modes Excited by Electrons. *Nat. Commun.* **2014**, *5*, 4125.

(54) Johnson, P. B.; Christy, R. W. Optical Constants of the Noble Metals. *Phys. Rev. B* **1972**, *6*, 4370–4379.

(55) Johnson, P. B.; Christy, R. W. Optical Constants of Transition Metals: Ti, V, Cr, Mn, Fe, Co, Ni, and Pd. *Phys. Rev. B* **1974**, *9*, 15.

(56) Maier, S. A. *Plasmonics: Fundamentals and Applications*; Springer US: New York, NY, 2007.

(57) Nahm, T. U.; Jung, R.; Kim, J. Y.; Park, W.; Oh, S.; Park, J.; Allen, J. Electronic Structure of Disordered Au-Pd Alloys Studied by Electron Spectroscopies. *Phys. Rev. B - Condens. Matter Mater. Phys.* **1998**, *58*, 9817–9825.

(58) Grant, A. W.; Hu, Q. H.; Kasemo, B. Transmission Electron Microscopy “windows” for Nanofabricated Structures. *Nanotechnology* **2004**, *15*, 1175–1181.

For Table of Contents Use Only

Optical property – composition correlation in noble metal alloy nanoparticles studied with EELS

Shima Kadkhodazadeh,*,† Ferry Anggoro Ardy Nugroho,‡ Christoph Langhammer,‡ Marco Beleggia,† Jakob B. Wagner†